*30th EPS Conference on Contr. Fusion and Plasma Phys., St. Petersburg, 7-11 July 2003 ECA Vol. **27A**, P-4.60*

Assessment of the derivation of the plasma rotation and ion temperature profiles from an ITER x-ray crystal spectrometer

L.C. Ingesson,[1] R. Barnsley,[2] A. Malaquias[3] and M. O'Mullane[4]

[1] *EFDA Close Support Unit – Garching, Boltzmannstraße 2, D-85748 Garching, Germany; also at FOM-Instituut voor Plasmafysica, Associatie Euratom-FOM, Trilateral Euregio Cluster, PO Box 1207, 3430 BE Nieuwegein, The Netherlands*

[2] *Department of Pure and Applied Physics, Queen's University Belfast, Belfast BT7 1NN, UK*

[3] *Associação Euratom/IST, CFN, Av. Rovisco Pais, 1049-001 Lisboa, Portugal*

[4] *Department of Physics, University of Strathclyde, Glasgow G4 0NG, UK*

INTRODUCTION

An x-ray crystal spectrometer is foreseen on ITER to determine ion-temperature and plasma-rotation profiles. In this paper, the achievable performance in deriving plasma parameters is assessed for an imaging set-up and a system consisting of discrete lines of sight; the importance of including an edge-viewing system is also investigated. Derivation of rotation and ion-temperature profiles from broad emission profiles on present-day magnetic fusion devices, using both active and passive visible and near-uv spectroscopy, has been reported in the literature [1–4]. For the present study in the x-ray range, a well-regularized reconstruction method was developed that can derive poloidal and toroidal rotation from signals that contain information on both.

SIMULATED X-RAY SPECTROMETER SIGNALS

Spectral line emission at wavelength λ_0 from a thermal plasma with a flow velocity $\boldsymbol{v}$ has, for small Doppler broadening and shift with respect to λ_0, the approximate line shape given by

$$\varepsilon(\lambda) = \frac{\varepsilon_0}{\sqrt{2\pi}\sigma_\lambda} \exp\left[-\frac{(\lambda - \lambda_0 - \lambda_D(\boldsymbol{v},\boldsymbol{l}))^2}{2\sigma_\lambda^2} \right], \qquad (1)$$

with line intensity ε_0 and Doppler broadening $\sigma_\lambda^2 = \lambda_0^2 k T_a / m_a c^2$ (k is the Boltzmann constant, c the velocity of light, T_a the temperature of the ion species, and m_a the atomic mass of the ion species). The Doppler shift depends on the magnitude and direction of the velocity field $\boldsymbol{v}$ with respect to the viewing direction $\boldsymbol{l}$ and is given by the inner product $\lambda_D = -(\lambda_0 / c)\boldsymbol{v}\cdot\boldsymbol{l}$. The quantities ε_0, $\boldsymbol{v}$ and σ_λ^2 are functions of location in the plasma and can be parameterized by the normalized minor radius ρ and angle θ on flux surfaces.

The ratio of line width to line shift in the spectral emission is small for heavy ions. Hence, for flow measurements it is preferable to measure the spectral emission of heavy ions (with a high-resolution spectrometer) rather than of light ions. In the x-ray region, emission profiles of heavy impurities are non-zero over a large part of the plasma cross-section. X-ray crystal spectroscopy can give the required accuracy for typical tokamak flow velocities and ion temperatures over this radial range. Figure 1 shows two possible geometries for x-ray crystal spectroscopy on ITER, which are tilted at a toroidal an-

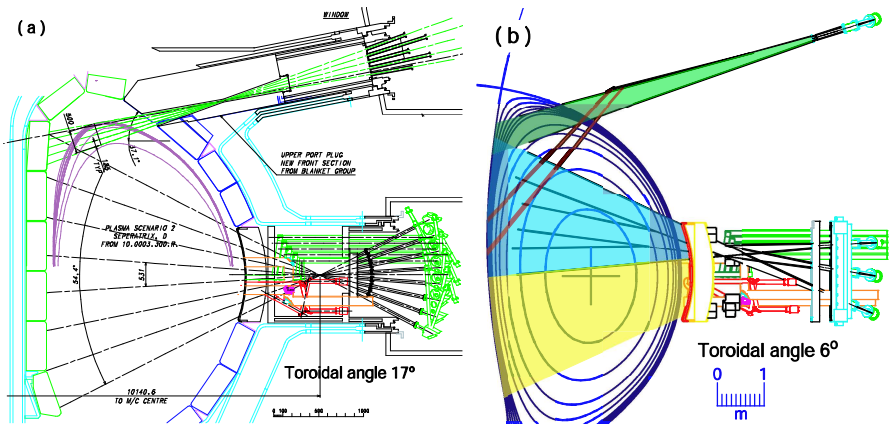

Figure 1: *Two possible implementations of lines of sight of x-ray crystal spectrometers on ITER. (a) Discrete lines of sight, tilted at* η = 17°. *(b) Imaging systems with semi-continuous coverage on detector arrays in the shaded areas (and two single channels; red), at* η = 6°.

gle η. Because the emissivity is non-zero over a finite region, inversion techniques have to be used to reconstruct the local emissivity from the line-integral measurements. Full tomographic reconstructions are not possible as the plasma can only be viewed from one direction (approximately horizontal lines of sight). We will assume that the quantities ε_0, v and σ_λ^2 are constant on flux surfaces, although the present inversion technique is generally applicable provided an accurate functional dependence on θ on flux surfaces is available from modelling or other measurements.

RECONSTRUCTION METHOD

If the flow velocity and hence Doppler shift is not negligible, the spectral line shape given by Eq. (1) varies along the measuring lines of sight due to the changing angle between the flow field and the line of sight. Therefore, emission profiles cannot be reconstructed independently for each wavelength. Techniques of so-called vector tomography [5–8] can reconstruct the scalar field (emissivity) and vector field (velocity) independently from spectrally resolved measurements from many directions.

It has been recognized [5–7] that linear equations, from which the required quantities can be solved, can be obtained by taking moments in λ of the (nonlinear) line integrals over Eq. (1), after the background has been subtracted. The simulations were performed in a cylindrical geometry (with radial variable ρ) because this simplifies the evaluation of the line integrals of Eq. (1) and their moments, while the present simulation results for centrally peaked emission will be largely representative of the actual geometries foreseen for ITER. This is because line integrals through a circular plasma are similar to those through the core of a vertically elongated plasma with similar minor radius a, and most effects can be directly studied or artificially simulated. For the cylindrical geometry the moments of the line integral $f(p,\lambda)$ at impact parameter p are

$$\mu_0(p) = \int_0^\infty f(p,\lambda)\,\mathrm{d}\lambda = 2\int_{|p|}^a \varepsilon_0 \frac{\rho}{\cos\eta\sqrt{\rho^2-p^2}}\,\mathrm{d}\rho\,, \tag{2}$$

$$\mu_1(p) = \int_0^\infty (\lambda-\lambda_0) f(p,\lambda)\,\mathrm{d}\lambda = 2\int_{|p|}^a \varepsilon_0\lambda_0\left[v_\mathrm{t}'\sin\eta - v_\mathrm{p}'\cos\eta\,\frac{p}{\rho}\right]\frac{\rho}{\cos\eta\sqrt{\rho^2-p^2}}\,\mathrm{d}\rho\,, \tag{3}$$

$$\mu_2(p) = \int_0^\infty (\lambda-\lambda_0)^2 f(p,\lambda)\,\mathrm{d}\lambda = 2\int_{|p|}^a \varepsilon_0\left\{\sigma_\lambda^2+\lambda_0^2\left[v_\mathrm{t}'\sin\eta - v_\mathrm{p}'\cos\eta\,\frac{p}{\rho}\right]^2\right\}\frac{\rho}{\cos\eta\sqrt{\rho^2-p^2}}\,\mathrm{d}\rho\,, \tag{4}$$

where ε_0, v_t', v_p' and σ_λ^2 are functions of ρ, and v_t' and v_p' are the toroidal and poloidal rotation velocities normalized to c. Note that the v_p' term in μ_1 will change sign with p (indicating rotation in or opposite to the viewing direction) and that for all quantities, except v_p, the mathematical formulation is that of the Abel integral. Arbitrary viewing geometries will yield similar, but more-complicated expressions or may have to be calculated numerically.

Inversion of μ_0 of Eq. (2) will give $\varepsilon_0(\rho)$. Inversion of μ_1 of Eq. (3) is straightforward if either v_t or v_p is negligible, if $\eta = 0$, or if even or odd components of $\mu_1(p)$ can be eliminated from symmetric measurement. Otherwise, v_t and v_p cannot be separated before reconstruction. We have developed a technique that approximates $v_\mathrm{t}(\rho)$ and $v_\mathrm{p}(\rho)$ iteratively. Inversion of μ_2 of Eq. (4) is straightforward, although the velocity term has to be subtracted from the result to yield $\sigma_\lambda^2(\rho)$ and $T_\mathrm{i}(\rho)$.

Because the inversion results of μ_1 depend on the reconstructed ε_0, and μ_2 on ε_0, v_t' and v_p', reconstruction errors may accumulate. For that reason it is very important to use a well-regularized reconstruction method [9]. We discretize Eqs. (2–4) on a regular grid in ρ with triangular basis functions. The grid was chosen sufficiently fine (50 points) so that the reconstruction result is independent of this choice. The discretization results in a matrix equation. We used a constrained optimization reconstruction method [10] with estimated measurement

error bars as constraint, and an objective functional that favours smoothness of the solution, flatness (or zeroness of v_p') at $\rho = 0$ and small size at the edge.

We have not taken into account the instrument function in this analysis, as it can be shown that a symmetric instrument function drops out of Eqs. (2–3) and modifies the second moment by a constant factor that depends on the instrument width.

SIMULATION RESULTS

Simulations were performed for a range of plasma and instrument parameters in a standard H-mode plasma ($n_e \sim 10^{20}$ m^{-3}, $T_e \sim 25$ keV) and a plasma (7×10^{19} m^{-3}, 27 keV) with internal transport barrier around $\rho = 0.6$. For the latter, the Kr line emission and the predicted v_t, v_p and T_i are shown as solid lines in Fig. 2. The simulated measurements include continuum radiation, a detection background level and Poisson noise. Line and continuum radiation were calculated with the ADAS database [11] and SANCO transport code. The reconstructed profiles of one of the simulations, including the iteratively separated v_t and v_p as described above, are shown as dotted lines in the same figures.

The results of Fig. 2 show that with an up-down symmetric imaging system (blue and yellow areas in Fig. 1(b)) with 35 lines of sight excellent reconstructions can be obtained for ε_0, and for T_i at $\rho < 0.6$ (for this particular ε_0). For plasmas with lower T_i or higher rotation velocities, however, the velocity term in Eq. (4) may not be negligible and the quality of the T_i reconstruction can depend on the accuracy of the reconstructed velocities. The quality of the reconstructed velocities in Fig. 2(b,c) is reasonable; the deviations from the input profile are due to the inability to accurately separate the symmetric and anti-symmetric components in the noisy μ_1. With parameters such as higher plasma rotation or higher signal levels (higher sensitivity or longer integration times), the velocity reconstructions are significantly improved. The poor quality of reconstructed velocities and T_i at $\rho > 0.6$ is an inevitable consequence of the division by poorly reconstructed small values for ε_0 (however, it should be possible to reconstruct these quantities for $\rho > 0.6$ from other spectral lines, e.g. of argon). The simulation of Fig. 2 was done with a rather high krypton concentration of 10^{-4} (leading to $\Delta Z_{eff} = 0.1$), but a short integration time (30 ms) and conservative sensitivity. Similar results were obtained with a concentration of 10^{-5} (with negligible ΔZ_{eff} and incremental total radiation power of about 0.5 MW) with an integration time of 1 s, or an improved sensitivity in the same proportion. Increasing the resolving power was shown not to have any effect, as the increased number of channels each receive fewer counts: these effects cancel out in the noise level of the moments. Although the poloidal velocity is small, it cannot be neglected in the reconstruction of the toroidal velocity.

Various other line-of-sight configurations have been investigated. Simulations have shown that an imaging system that views only the top half of the plasma (blue area in Fig. 1(b)) is inadequate unless v_p is negligible, as the contributions of v_t and v_p cannot be separated, even for favourable signal levels or large rotation velocities. If v_t is negligible, or the system is at

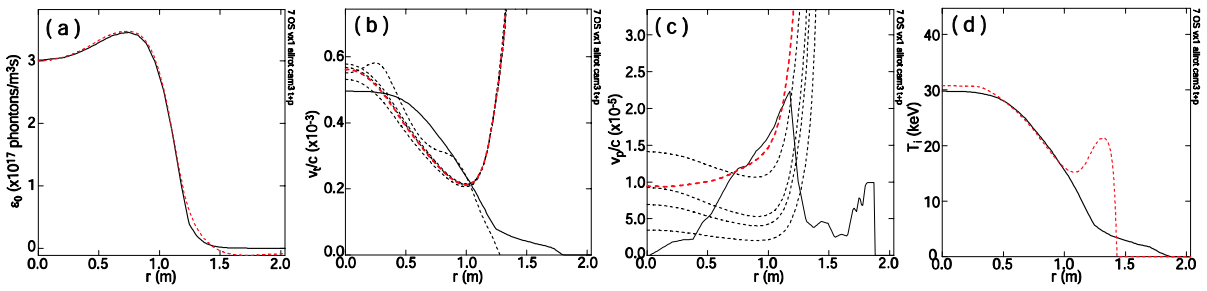

Figure 2: *Simulation results for an ITER plasma with an internal transport barrier and a Kr concentration of 10^{-4}, measuring the spectral line at 0.945 Å with an integration time of 30 ms, sensitivity 1.4×10^{-7} cm^2 and dispersion 0.019 pm/channel with the imaging system covering both the top and bottom core of the plasma. (a) Emission profile, (b) toroidal and (c) poloidal rotation velocities, and (d) ion temperature. Solid lines: input data. Red dotted lines: reconstructed profiles. Black dotted lines (b,c): iterative approximation.*

$\eta = 0$, the reconstruction of v_p is still rather poor for the reference conditions described above; significant improvements are obtained, however, for larger values of v_p or more signal. Discrete lines of sight as in Fig. 1(a) give significantly worse reconstruction results than the imaging system discussed in the previous paragraph, although under more favourable signal levels the results may be acceptable. An important conclusion is that for relatively broad emission profiles, the discrete system requires an edge view (green lines in Fig. 1(a)) to bound the values at the edge, as this significantly improves the reconstruction. For the imaging system however, the availability of an edge view (green area in Fig. 1(a)) has little impact even though the lines of sight do not cover the entire profile (such an edge system can be used to view other spectral lines). The number of lines of sight used in the imaging system is not very important, as long as it is over 20 (the sensitivity is inversely proportional to the number of lines of sight). The number of lines of sight of the discrete system (8) are very marginal.

In addition to the plasma with internal transport barrier described, simulations were performed for an H-mode plasma. The results are worse than Fig. 2, as T_i, v_t and v_p are all smaller. For the discrete system, the T_i determination is poor for the given signal levels, whereas for the up-down symmetric imaging system it is acceptable.

DISCUSSION AND CONCLUSIONS

The simulation results demonstrate that with the instrument design foreseen and in suitable plasma conditions, the present analysis technique can provide the core T_i within the ITER measurement requirements (100ms time resolution, $a/10$ spatial resolution, 10% accuracy). The situation is more complicated for the velocity reconstructions, as these are very noise sensitive. Accurate determination of these is on the edge of feasibility given instrumental factors (such as the size and reflectivity of the crystal), required Kr concentration and the rotation velocities expected for ITER (which are low in comparison with present machines). Realistic spatial and time resolution is below the ITER measurement requirement (10 ms, $a/30$). Without detailed simulations it is very complex to predict the performance for any given situation as the system operates in a parameter range in which performance critically depends on many parameters: line emission strength, radial extent of the line emission, T_i, rotation velocities, continuum radiation, signal level, and the line-of-sight lay-out.

Future simulations should address several issues: camera configurations in which symmetry can help the separation of v_t and v_p, testing the sensitivity to uncertainties in position and the shape of flux surfaces, the effect of beam widths and the instrument function, inclusion of toroidal and poloidal rotation in a toroidal D-shaped plasma, and models for variations of quantities on flux surfaces (e.g. variation of not only direction but also magnitude of $\boldsymbol{v}$ on flux surfaces in toroidal geometry, and variation of ε_0 due to the centrifugal force on heavy impurities). In addition, alternative spectral lines could be investigated (high intensity at low concentrations with overall low total radiated power), including more narrow and broader profiles. The prospect on constraining the reconstructed profiles to T_i, v_t and v_p for $\rho > 0.6$ determined from other spectral lines with suitable emission profiles should also be considered, for instance by implementing the constrained-optimization method described in Ref. 12.

ACKNOWLEDGEMENTS

The authors wish to thank Dr. A. Loarte for providing ITER profiles. This work has been conducted under the European Fusion Development Agreement.

[1] R.S. Shaw, J. Opt. Soc. Am. A **4**, 2254 (1987)
[2] R.E. Bell, Rev. Sci. Instrum. **68**, 1273 (1997)
[3] I. Condrea *et al.*, Phys. Plasmas **7**, 3641 (2000)
[4] R.P Golingo *et al.*, Rev. Sci. Instrum. **74**, 2332 (2003)
[5] J. Howard, Plasma Phys. Control. Fusion **38**, 489 (1996)
[6] A.L. Balandin *et al.*, Eur. Phys. J. D **17**, 337 (2001)
[7] N.P. Efremov *et al.*, J. Quant. Spectrosc. Radiat. Transfer **53**, 723 (1995)
[8] G. Fuchs *et al.*, Plasma Phys. Control. Fusion **40**, 91 (1998)
[9] M. Bertero *et al.*, Inverse Problems **4**, 573 (1988)
[10] L.C. Ingesson *et al.*, Rev. Sci. Instrum. **71**, 1370 (2000)
[11] H.P. Summers, *Atomic Data and Analysis Structure User Manual (2nd Edition, 2001)*; available from http://adas.phys.strath.ac.uk
[12] G.C. Fehmers *et al.*, Inverse Problems **14**, 893 (1998)